ENHANCED PERFORMANCE OF PHOTOVOLTAIC MODULES VIA EXPERIMENTAL EVALUATION OF NOVEL HEAT SINK DESIGNS

Abdel-Halim Saber Salem Said[1,2*], Anas Ahmed[3], A. Fouda[1,4], H. F. Elattar[1]

[1] Department of Mechanical and Materials Engineering, Faculty of Engineering, University of Jeddah, Jeddah 23890, Saudi Arabia.

[2] Mechanical Power Engineering Department, Faculty of Engineering, Zagazig University, Zagazig 44519, Sharkia, Egypt

[3] Department of Industrial and Systems Engineering, Faculty of Engineering, University of Jeddah, Jeddah 23890, Saudi Arabia

[4] Department of Mechanical Power Engineering, Faculty of Engineering, Mansoura University, 35516 El-Mansoura, Egypt

* Corresponding author email: asssaed@uj.edu.sa

This study investigates the performance of photovoltaic (PV) module integration with novel designs of heat sink modules (PV/HS-I, PV/HS-II, PV/HS-III, and PV/HS-IV), introducing an optimized converging-diverging fin configuration (PV/HS-II) that demonstrates superior cooling performance under extreme desert conditions. The experimental work analyzes the impact of cooling air velocity, solar intensity, solar panel surface area, and power temperature coefficient on the PV module performance and productivity. The results demonstrate that raising the cooling air speed enhances convective cooling, lowers the temperature of the PV surface, and increases electrical efficiency and productivity, especially for the PV/HS-II design, which is the most effective design compared to other heat sink configurations. Under Jeddah's climatic conditions, the PV/HS-II module achieves a peak electrical efficiency of 19.5% and the highest electrical energy productivity of 65.57 kW. The decrease in power temperature coefficient from -0.5 %/°C to -0.3 %/°C increases electrical efficiency from 16.5 % to 18.65 %, improving electrical energy productivity by 40 %. This work provides the first comprehensive experimental evaluation of fin geometry optimization for PV cooling in high-irradiance environments, offering practical design solutions for solar farms in hot climates. The study shows how crucial active cooling is for reducing efficiency losses, especially in places with a lot of sunlight, like Jeddah, Saudi Arabia. It also gives valuable tips for improving the performance of photovoltaic systems.

Keywords: *PV electrical efficiency; innovative heat sinks, electrical energy productivity; solar intensity; power temperature coefficient.*

1. Introduction

Global energy demand and fossil fuel pollution have increased the need for alternative energy sources like photovoltaics. Barriers to the full deployment of renewable energy resources to replace fossil resources are discussed [1]. PV systems, which use semiconductor materials to turn sunlight into electricity, are a renewable and environmentally beneficial way to address rising energy needs [2]. PV technology struggles with low conversion efficiency due to dust [3], reflection, shade, and temperature [4]. Photovoltaic cells convert only visible light into electrical energy, while the rest, notably infrared light, is converted into thermal energy. This extra heat can damage PV panels, lowering their efficiency and lifespan [5] of different types of PV cells, considering the effect of TPT layer absorptivity [6]. This difficulty has led researchers worldwide to create unique cooling solutions to improve PV panel efficiency and longevity. This has led to the development of natural, passive, and sophisticated liquid cooling and forced convection cooling technologies. Many solar cooling studies have focused on specialized cooling methods. Solar cells cooled with a heatsink and nanofluid added with aluminum nanoparticles [7], using phase change material [8], using hydraulic cooling [9], integration with a passive Multi-layered PCMs cooling system [10], and a hybrid photovoltaic thermal system through parallel water pipe integration [11]. Research has examined water-based cooling technologies, passive multi-layered PCM cooling systems, heatsinks using nanofluid enhanced with Aluminum nanoparticles, and parallel water pipe integration. Siah Chehreh Ghadikolaei [12] reviewed cooling technologies, while Cui et al. [13] evaluated phase change PV/T systems, considering external, energy, economic, and environmental variables. Madhi et al. [14] examined nanofluid thermo-PV system performance in energy, electricity, economics, and the environment. Dida et al. [15] examined mono and hybrid nanofluid photovoltaic/thermal cooling systems. This discovery could change PV system cooling tactics, making solar energy a viable and sustainable energy source for the future. Photovoltaic (PV) systems turn sunshine into electricity as an alternative to grid power. However, these systems generate heat, raising cell temperature and decreasing efficiency [16]. Phase-change materials have been developed to improve solar efficiency, as have water- and air-cooling methods. Using cooling ducts, heat sinks, and air collectors, forced convection is combined with radiative cooling [18], phase change materials, nanofluids [19], thermoelectric systems, heat pipes, heat pumps, and other advanced techniques [20]. Heat reduces PV panel efficiency in high-temperature situations, especially deserts and tropical regions with high midday temperatures. Use low-temperature coefficient PV panels in such settings. Cooling equipment with adequate airflow reduces the impact of high temperatures on solar panel efficiency. By adjusting the rib-base plate angle, A computational approach using air-cooled heat sinks to reduce PV temperatures was presented by Popovici et al. [21]. ANSYS-Fluent created a turbulent flow model showing PV panel average temperature reduction under multiple configurations. Passive photovoltaic cooling [22,23] uses air, water, or conductive materials [24,25] to dissipate heat without energy consumption. Pumps or fans circulating water, air, or nanofluids enhance cooling, heat conduction, and energy efficiency. Due to their thermal conductivity, aluminum heat sinks cool PV panels well [26]. Foam or fin configurations, along with other aluminum-based cooling methods [27], lower surface temperature and enhance electrical efficiency. Almuwailhi and Zeitoun [28] found that natural, forced, and evaporative cooling solar panels increase efficiency and energy output. In-depth discussion is given of solar panel cooling, including forced convection via cooling ducts, heat sinks, air collectors, and passive and active cooling systems. Performance enhancement attempts on the photovoltaic/thermal module are reviewed [29], and a new photovoltaic panel cooling classification system [30,31]. A comprehensive review of cooling, concentration, spectral splitting, and tracking techniques is presented [32].

Al-Waeli, Ali H.A. et. Al. [33] compared nanofluid and nano-PCM cooling methods for PV/T systems using mathematical and neural network models, showing that the prediction models effectively enhance system

performance with low error rates. Kazem, Hussein A. et. al. [34] showed that SiC nanofluid notably boosts PV/T system performance over water-based and conventional setups, proving effective in Oman's climate. Djordjevic, Stevan N. et. al.[35] simulated a closed-loop water cooling system applied to the back of a PV panel. Their results show increased power output by 41.75% by significantly lowering panel temperature, with simulations confirming its effectiveness and accuracy under real weather conditions. The experimental study of Muniy, Srilasri, and Narayanasamy, Stalin [36] shows that using Al_2O_3 nanofluid (0.04% concentration) at a 40 Lph flow rate improves the thermal and electrical efficiency of PV modules compared to deionized water.

Photovoltaic (PV) systems suffer significant efficiency drops in high-temperature environments, especially in sun-rich regions like Jeddah. Although many cooling methods have been explored, such as passive heat sinks, nanofluids, and phase-change materials, current research often overlooks the combined optimization of heat sink design, airflow patterns, and temperature coefficient effects in real-world conditions. This gap limits the development of affordable, scalable cooling solutions for harsh climates. This work presents an experimental evaluation of four innovative heat sink designs (PV/HS-I to IV) that feature unique fin configurations. These designs aim to optimize heat dissipation, reduce solar cell temperatures, and increase electrical efficiency by controlling airflow speeds (0.5–3 m/s), adjusting sun intensities (1020–5102 W/m²), and modifying power temperature coefficients (-0.5 to -0.3 %/°C). By carefully analyzing these variables along with solar panel surface area and air mass flow rates, we seek to find the best setup for next-generation photovoltaic systems in Jeddah's challenging environment. This approach links theoretical cooling methods with real-world implementation, offering insights into both energy efficiency and economic benefits in solar applications.

2. Heat sinks design and integration with PV

The main source of air heat is PV panels. These panels successfully recover waste heat from photovoltaic electricity generation using experimentally improved heat sinks. The recovered heat effectively warms the surrounding air, reducing the need for additional heating. Figure 1-a illustrates how the battery stores PV-generated energy electricity.

This section explains the physical models of the recommended heat sinks, which are designed to create integrated PV-HS modules by aligning the base temperature with the PV temperature. Modules utilize various heat sink designs for PV systems. Experimental plate and pin-fin shapes were tested in multiple configurations to enhance heat sink design. As shown in Fig. 1-b, four heat sink shapes were tested for thermal performance. Evaluation of heat sink configurations includes:

- HS-I: Perforated plate fin-tilted square pin fin.
- HS-II: Conv/div perforated plate-tilted square pin fin.
- HS-III: Corrugated perforated plate-tilted square pin fin.
- HS-IV: Parallel perforated plate-tilted square pin fin.

After evaluating market availability and pricing, Aluminium Alloy 6061 was chosen for heat sink modules. The selected aluminum alloy has a specific heat capacity of 897 J/(kg·K), a melting point of 585°C, and a thermal conductivity of 202 W/(m·K). All variants featured 5 plate fins and 32 pin fins, maintaining identical volume and fin count. The heat sink dimensions were 14 cm × 14 cm × 13.2 cm (length × width × height). The plate fins are 4 mm thick and 120 mm tall. As shown in Fig. 1-b, all heat sinks measure 140 × 140 × 12 mm. Based on previous studies, this research carefully determined heat sink specifications, including fin spacing and length [37,38]. Each configuration was tested for thermal performance at different air velocities. This method assessed each design's performance under various operating conditions, indicating their suitability for advanced PV panels in solar power systems.

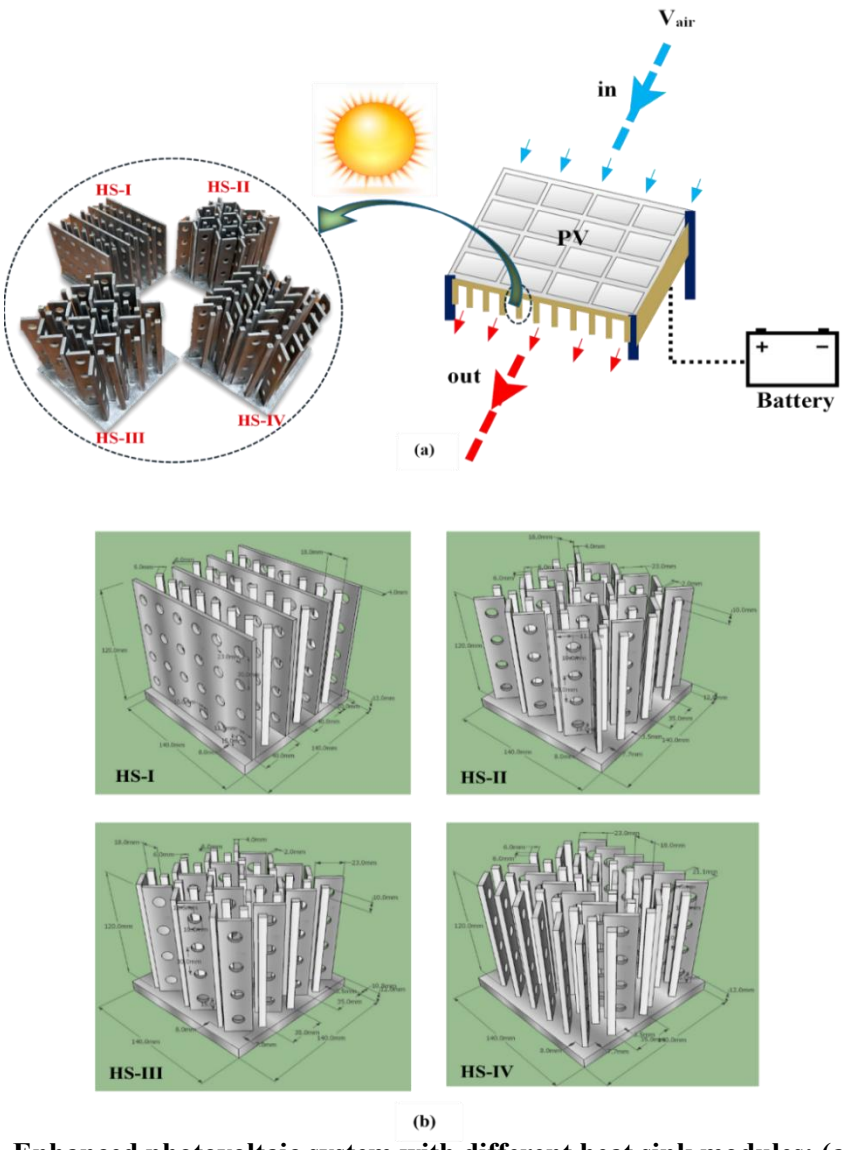

Figure 1. Enhanced photovoltaic system with different heat sink modules; (a) schematic of photovoltaic integrated system, (b) heat sink modules' dimensions

3. Methodology

3.1. Testing and measuring equipment

An experimental setup evaluated each heat sink design under various operational conditions to improve their compatibility with advanced photovoltaic panels in solar power systems. Figure 2 shows the experimental setup and heat sink modules in both photos and diagrams. The setup includes a wind tunnel, test section, heat sink modules, and measurement and control devices. The 1500-mm vertical wind tunnel connects the airflow inlet to the exhaust fan. The flow channel has a hydraulic diameter (D_h) of 150 mm, based on its 150 mm by 150 mm square cross section. To achieve enough air velocity for testing, a 0.18 m by 0.18 m fan with a variable-speed motor (70 W) was installed at the outlet. A 250 W dimmer-controlled fan provides precise airflow velocity. To ensure even airflow in the test area, the wind tunnel features a 3D-printed honeycomb structure at the intake. A 10 cm by 15 cm honeycomb helps streamline airflow before entering the duct.

The heat sink is positioned 80 cm from the channel inlet in the test section. Different heat sinks were heated using a 14 cm by 14 cm flat electric heater with a power output of 300 W. A variac adjusted the voltage precisely to simulate a hybrid system's solar heat input. At the same time, a wattmeter recorded the heater's

output. Thermally conductive epoxy bonded the heater to the heat sink models for better heat transfer efficiency. The base plate and heater assembly were insulated with 1.2 cm-thick rock stone insulation to minimize heat loss and placed on a hardwood support measuring 18.7 cm × 16.2 cm × 5 cm. A hollow part within the wooden support housed the heat sink base, exposing only the upper section to the airflow in the wind tunnel. Anemometers measured the air velocity in the wind tunnel. The average air velocity was measured 500 mm from the inlet with a flow sensor. The setup accurately measured airflow parameters, with a velocity range of 0.1 to 25 m/s and a temperature range of 0°C to 50°C. A digital manometer measured the pressure drop over the heat sink. Airflow resistance was assessed at pressure ports located 20 mm from both the inlet and outlet of the heat sink module.

Fourteen K-type thermocouples are used to measure temperature. T1 and T2 record the average air temperatures at the input and output. The thermocouples, positioned 150 mm from the heat sink's inlet and outlet, measure the output air temperatures perpendicular to the airflow. The insulation and wooden base holder contain three additional thermocouples (T3, T4, and T5) to evaluate heat dissipation from the heater. Figure 2-c shows nine thermocouples (T6–T14) that measure the average surface temperature of the heat sink. This setup enabled precise regulation and measurement of thermal parameters for assessing the heat sink's thermal performance. Data was collected using a National Instruments compact DAQ USB chassis and a 16-channel C Series Temperature Input Module. A computer acquired thermocouple signals from the DAQ system via LabVIEW. LabVIEW displayed real-time data from the acquisition system. The graphical programming environment visualized temperature distribution, evaluated heat sink performance, and exported data for further analysis. Its user-friendly interface allowed for the creation of temperature maps, heat transfer graphs, and reports, thus enhancing experimental efficiency. The tests employed heat inputs of 20, 60, and 100 W, resulting in heat fluxes of 1020, 3061, and 5102 W/m². Air velocities increased by 0.5 m/s, ranging from 0.5 to 3 m/s. Accurate control and measurement of thermal and airflow parameters demonstrated that the heat transfer efficiency of the heat sink arrangement is improved. Table 1 outlines the specifications of the measurement instruments used in the experiment setup.

3.2. Conditions and experimental procedure

For a stable state and reliable readings, follow this approach and experimental program:

- Position the heat sink module of the wind tunnel safely 800 mm from the intake.
- Use the dimmer to adjust the fan speed for air velocity.
- Set the air velocity to 0.5, 1, 1.5, 2, 2.5, or 3.0 m/s.
- Adjust heater power with a variable AC power transformer to achieve the required input: 20, 60, or 100 W.
- Allow 30–60 minutes for steady-state conditions to establish, depending on air velocity and heat input.
- Measure thermocouple readings at heat sink sites, including input and output air temperatures (T1 and T2) and surface temperatures at various locations. LabVIEW captures real-time thermocouple data from a data acquisition system.
- Use LabVIEW to monitor and analyze heat sink temperature distributions in real time, and store data for further analysis.
- Verify wind tunnel air velocity with a hot wire anemometer.
- Repeat the steps for each combination of air velocity and thermal input within the specified ranges:
  - Air velocity: 0.5 to 3.0 m/s (increments of 0.5 m/s)
  - Heat inputs: 20 W, 60 W, 100 W

This systematic approach ensures accurate assessment of each heat sink module's thermal performance and airflow characteristics within the DAQ system and LabVIEW software, enabling reliable data collection and comprehensive analysis.

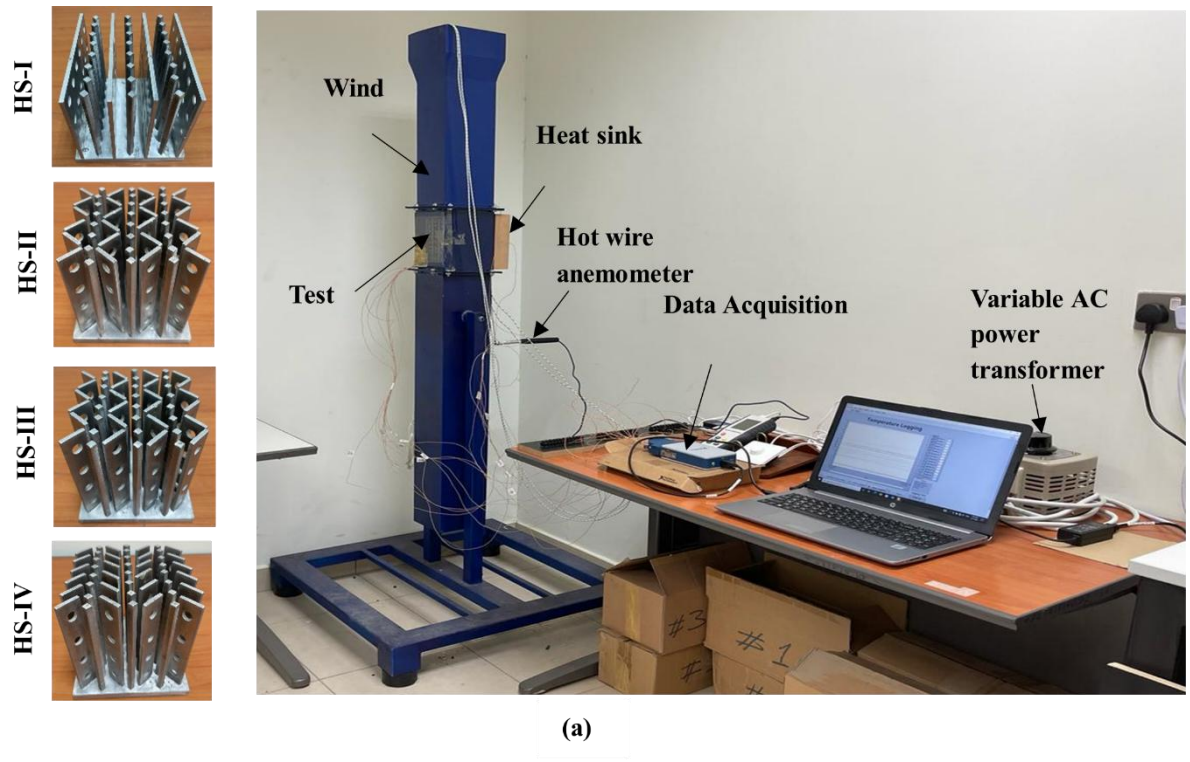

Figure 2. Experimental configuration: (a) actual photographs, (b) schematic representation, (c) thermocouple placement on the photovoltaic-heat sink module

Table 1. Measurement Instruments and Specifications

Device	Function	Operating Range	Precision / Error Margin	Measurement Resolution
Type K Thermocouple	Temperature sensing	-180°C to 105°C	±2.2°C	0.1°C
Hot Wire Anemometer	Air velocity measurement	0.1 m/s to 25 m/s	±3% of the measured value	0.01 m/s
	Ambient temperature measurement	0°C to 50°C	±1°C	0.1°C
Digital Manometer	Pressure drop assessment	0 to 2000 Pa	±1.5% of full scale	1 Pa
Dimmer	Fan power regulation	Up to 250 W	±5%	Not applicable
Variable AC Power Transformer	Heater voltage and power control	0–150 V / Up to 1500 W	±1%	1 V
DAQ System	Multi-sensor temperature acquisition	-50°C to 200°C	±0.1°C	0.01°C

3.3. Processing and Reduction of Data

The following equations are used in the HS modules' data reduction and processing.

The HS module's energy balance formulas

$$\dot{Q}_{a,HS} = \dot{Q}_H - \dot{Q}_L \quad (1)$$

$$\dot{Q}_{a,HS} = \dot{m}_{a,HS} c_{p,a} (T_2 - T_1) \quad (2)$$

The rate of air mass flow across the HS module is determined using

$$\dot{m}_{a,HS} = \rho_{air} A_c V_{air} \quad (3)$$

The total loss of heat transfer via the HS modules is calculated by

$$\dot{Q}_L = \frac{T_4 - T_3}{R_t} \quad (4)$$

T_3 and T_4 represent the internal and external temperatures of the wooden box surface (refer to Fig. 2 (c)), whereas R_t denotes the overall thermal resistance of the wooden box, which may be computed as

$$\frac{1}{R_t} = \sum_{i=1}^{n} \frac{1}{R_i} \quad (5)$$

Where R_i represents the cumulative heat resistance of the HS module's wooden housing:

$$R_i = \frac{x_i}{k_{wood} A_i} \quad (6)$$

x represents the thickness of the wooden box sides, whereas k denotes the thermal conductivity. The mean surface and base temperatures of the HS module are derived from Equations (7) and (8).

$$T_{s,HS} = \frac{\sum_{i=6}^{14} T_i}{9} \quad (7)$$

$$T_{b,HS} = \frac{\sum_{i=6}^{9} T_i}{4} \quad (8)$$

where *i = 6, 7, …, 14 represents* the locations of thermocouples scattered around the HS module surface

The air mass flow rate via the PV-HS module is determined by:

$$\dot{m}_{air} = \rho_{air} A_c v_{air} N_{p,HS} \quad (9)$$

The area of the PV is determined as

$$A_{PV} = A_{b,HS} N_{p,HS} N_{s,HS} \quad (10)$$

$N_{p,HS}$ and $N_{s,HS}$ denote the quantities of heat sink modules arranged in parallel and series, respectively. The efficiency of photovoltaic (PV) systems is ascertained in the following manner.

$$\eta_{el} = \eta_{ref} - \beta(T_{PV} - T_{ref}) \quad (11)$$

where η_{ref}= 20% at T_{ref}= 25 °C

The electrical energy generated can be computed as follows

$$E_{el} = \eta_{el} I_s A_{PV} \quad (12)$$

The equations above are resolved numerically utilizing EES software. Electrical efficiency, power generation, and cooling air flow rate are addressed in EES software V. 10.561 [39]: Tab. 2 lists operational and design parameter ranges.

Table 2. Values and ranges of studied and operational parameters

Parameter	Values / Ranges
Ambient Temperature ($t_{a,o}$)	26 °C
Heat Sink Module Designs	Four PV-integrated heat sink configurations: PV/HS-I, PV/HS-II, PV/HS-III, PV/HS-IV
Solar Irradiance (I_s)	1020, 3061, 5102 W/m²
Cooling Air Velocity (V_{air})	0.5, 1.0, 1.5, 2.0, 2.5, 3.0 m/s
Air Mass Flow Rate ($\dot{m}_{air}$)	0.54, 1.08, 1.62, 2.16, 2.70, 3.24 kg/s
Photovoltaic Surface Area (A_{PV})	30 m² to 100 m² (in 10 m² increments)
Power Temperature Coefficient (β)	0.25%/°C to 0.5%/°C (in 0.05%/°C steps)

Engineering Equation Solver (EES) is a powerful software application designed for solving complex nonlinear equations in thermodynamics, heat transfer, and fluid mechanics. Recent studies demonstrate its effectiveness in addressing technical problems. EES uses fluid thermodynamic and transport property data from the National Institute of Standards and Technology (NIST), a global authority. EES calculates enthalpy, entropy, and specific heat using NIST's accurate and experimentally validated data.

3.4. Analysis of uncertainty

Experimental error from measurements and estimated variables must be evaluated. Moffat [40] and Taylor [41] employ source errors of experimental variables such as temperature, air velocity, heat capacity, and others to assess uncertainty. The equations (1) to (12) can be expressed as $Y = f(X_1, X_2, X_3..., X_n)$.

The experimental uncertainty is calculated utilizing Equation (13):

$$U = \sqrt{\sum_{i=1}^{n} \left(\frac{\partial Y}{\partial X_i} . U_{X_i} \right)^2} \quad (13)$$

U indicates overall uncertainty, U_{Xi} represents the *i-th* measured variable uncertainty, and $\partial Y/\partial X_i$ is determined using numerical differentiation using a customized algorithm. Table 3 lists the estimated parameters' minimal and maximum uncertainty.

Table 3. Calculated parameters' uncertainty

Parameter	T_s	$\dot{m}_{air}$	η_{el}	$\dot{E}_{el}$
Min. uncertainty (%)	±0.4	±1.0	±1.2	±1.5
Max. Uncertainty (%)	±1.2	±3.5	±4.5	±5.2

4. Results and Discussions

This section will describe the performance of solar cells with new heat sink modules to lower solar cell surface temperatures and increase electrical energy generation efficiency. The effects of solar panel surface area (A_{PV}), cooling air velocity (V_{air}), solar intensity (I_s), power temperature coefficient (β), and air mass flow rates ($\dot{m}_{air}$) on solar panel surface temperature (T_{PV}), electrical efficiency (η_{el}), and electrical energy productivity ($\dot{E}_{el}$) in four heat sink configurations (PV/HS-I, PV/HS-II, PV/HS-III, and PV/HS-IV). Comparing novel heat sink modules simplifies efficiency evaluation. A Jeddah, Saudi Arabia, case study provides crucial new information about how heat sink integration improves solar energy systems in real-world scenarios.

4.1. PV/HS performance assessment and evaluation

4.1.1 Effects of cooling air velocity on PV electrical efficiency and temperature (Diff modules)

Figure 3-a shows how cooling air velocity (V_{air}) affects PV cell base surface temperature (T_{PV}) in four PV/HS configurations: PV/HS-I, II, III, and IV. As seen in Fig. 3, all heat sink module designs have lower T_{PV} as V_{air} rises. This graph illustrates that increasing v_{air} enhances convective cooling, lowering PV surface temperature. From 0.5 to 1.5 m/s, vair lowers T_{PV}, but up to 3 m/s, it has less effect. Its lowest T_{PV} at all V_{air} makes PV/HS-II the most efficient cooling design among the four PV/HS setups. Thus, the PV/HS-II module is the best for lowering PV cell base surface temperature (T_{PV}), improving PV performance and longevity. As seen in Fig. 3, raising V_{air} from 0.5 to 3 m/s reduced T_{PV} by 10% (from 29.5 to 26.5°C).

Figure 3-b shows that raising V_{air} from 0.5 m/s to 1.5 m/s improves PV electrical efficiency (η_{el}) modules for all module configurations. This is due to Fig. 3's T_{PV} drop. At V_{air} = 0.5 m/s, PV/HS-I has the lowest (η_{el} ≈17.9%) due to its maximum T_{PV} (≈32.2°C). PV/HS-II has the best efficiency (η_{el} ≈18.65%) because to its superior cooling and lower operating temperature (≈26.5 °C). As V_{air} climbs to 3 m/s, PV/HS-II has the greatest (η_{el} of 19.5%), followed by IV, III, and I. Improved convective cooling boosts PV efficiency, and PV/HS-II is the best combination with the lowest T_{PV} and highest η_{el}.

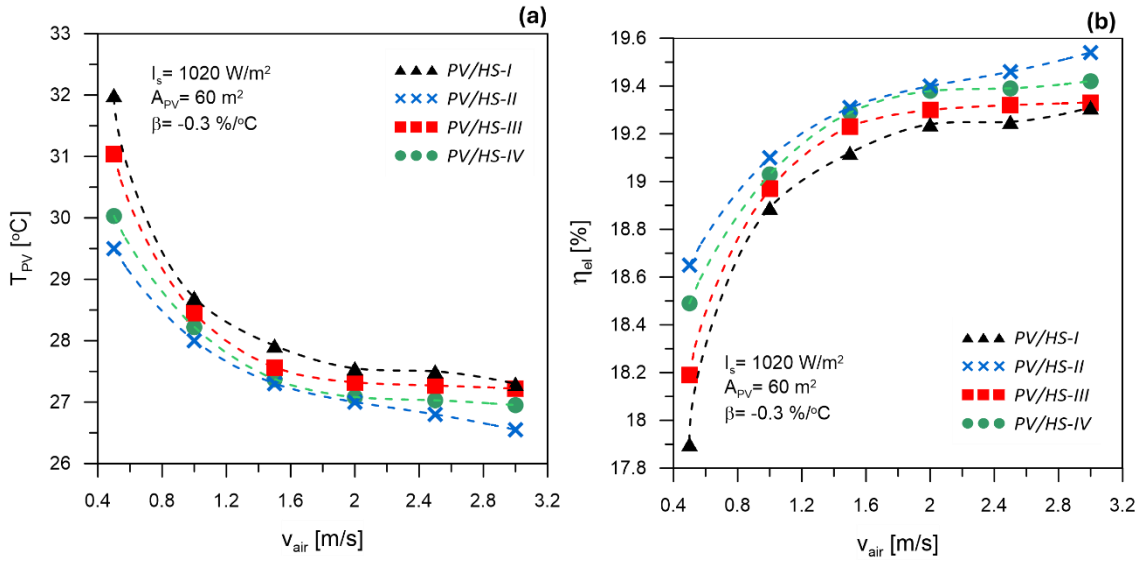

Figure 3. Effects of cooling air velocity on: (a) photovoltaic temperature, (b) photovoltaic electrical efficiency.

4.1.2 *Effect of cooling air velocity on PV electrical efficiency enhancement (Diff modules)*

Figure 4 demonstrates how V_{air} affects PV electrical efficiency enhancement ($\eta_{el,enh}$) of three PV/HS configurations (PV/HS-II, III, and IV) compared to PV/HS-I. Figure 4 demonstrates that the maximum ($\eta_{el,enh}$) occurs at V_{air}= 0.5 m/s for PV/HS-II, which improved by 4.25 %, followed by PV/HS-IV (3.3%) and PV/HS-III (1.7%). PV/HS-II and PV/HS-IV modules have far lower T_{PV} than PV/HS-I, which explains this considerable improvement at low V_{air}. $\eta_{el,enh}$ declines and levels off as V_{air} climbs from 1 to 3 m/s. At greater V_{air}, the cooling performance differential between PV/HS systems decreases, reducing ($\eta_{el,enh}$).

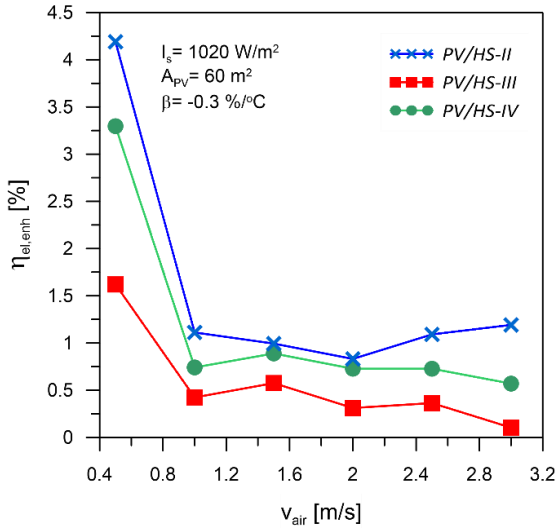

Figure 4. Influence of cooling air velocity on photovoltaic electrical efficiency enhancement.

4.1.3 *Impact of power temperature coefficient (β) on PV electrical efficiency*

Figure 5 exhibits the effects of V_{air} on PV/HS-II module (η_{el}) at varied power temperature coefficients (β). Figure 5 illustrates that as β decreases, the η_{el} rises, as the higher β, the more negative its impact on η_{el} increases, as the PV cell's η_{el} depends on the T_{PV}. Fig. 3-b shows that for V_{air}= 0.5 m/s, the η_{el} increases from 16.5 % to 18.65 % as β (from -0.5 %/°C to -0.3 %) decreases. As shown in Fig. 5, β decreases the η_{el} as V_{air} increases up to 3 m/s. Higher airflow enhances heat dissipation, reducing PV temperature and reducing the impact of β on η_{el}.

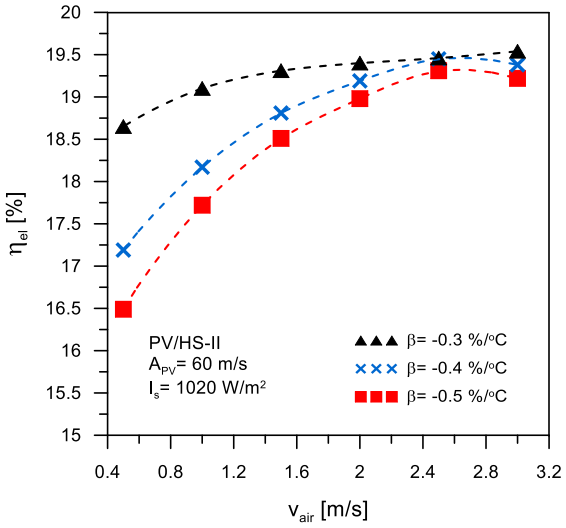

Figure 5. Effect of cooling air velocity on photovoltaic electrical efficiency at different power temperature coefficients

4.1.4 *Influence of solar intensity vs air velocity and mass flow rate*

Figure 6 illustrates the effect of V_{air} and $\dot{m}_{air}$ on the η_{el} of the PV/HS-II module under three different solar radiation intensities (I_s=1020, 3061, and 5102 W/m^2). As shown in Fig. 6, increasing V_{air} and $\dot{m}_{air}$ leads to improved η_{el} due to better cooling, which reduces the cell surface temperature. However, a clear inverse relationship is observed between I_s and η_{el}, as the η_{el} increases, the η_{el} decreases, even under the same cooling conditions. For instance, at I_s=1020 W/m^2, the η_{el} ranges from approximately 18.65% to 19.5%; at I_s=3061 W/m^2, it decreases to 14 %–17 %; and at the highest radiation level, I_s =5102 W/m^2, it drops further to 9 %–14 %. This means the η_{el} declines by ≈ 19 % when I_s increases from 1020 to 3061 W/m², and by an additional 39.5 % when it increases further to 5102 W/m². The drop is because T_{PV} increases with increasing I_s, which makes the PV solar cells work worse. So, to keep performance up, good cooling is quite essential, especially under intense solar conditions.

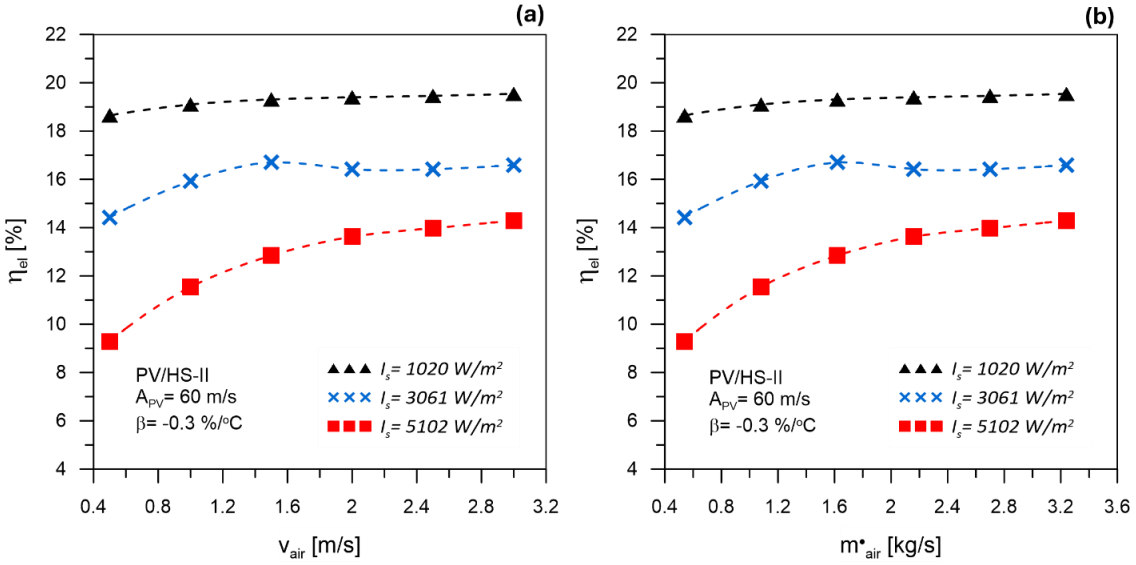

Figure 6. Photovoltaic electrical efficiency at different solar intensities with varying (a) cooling air velocity, (b) cooling air flow rate.

4.1.5 *Effect of PV area on system's productivity (electrical energy generated)*

Table 4 displays the effect of V_{air} on PV/HS module electrical energy productivity ($\dot{E}_{el}$) at A_{PV}= 60 m^2, β= -0.3%/°C. The table shows that boosting the V_{air} decreases T_{PV} and raises $\dot{E}_{el}$ for all PV/HS module setups. At V_{air}= 3 m/s, PV/HS-II module yields the maximum $\dot{E}_{el}$ of 11.96, 30.47, and 43.73 kW at I_s= 1020, 3061, and 5102 W/m2. The statistics demonstrate that air cooling considerably boosts PV module $\dot{E}_{el}$, and higher V_{air} improves performance even further. This highlights the importance of heat control, especially in solar-heavy environments. PV/HS-II has the highest $\dot{E}_{el}$ for all V_{air}, followed by PV/HS-IV, III, and I.

Table 5 and Fig. 7 demonstrate how A_{PV} impacts the system's electrical energy productivity ($\dot{E}_{el}$) at various sun intensities (I_s =1020, 3061, and 5102 W/m2) for PV/HS modules. $\dot{E}_{el}$ linearly rises with A_{PV}, as shown in Fig. 7. This is predicted as a larger A_{PV} captures and converts more I_s to electricity. At the same A_{PV}, the PV/HS-II module with a higher I_s of 5102 W/m^2 yields higher $\dot{E}_{el}$ than those with I_s =1020 and 3061 W/m^2. A_{PV}= 30 m² yields 19.67 kW $\dot{E}_{el}$ at I_s = 5102 W/m^2, up from 15.35 kW at I_s = 3061 W/m^2 and 5.909 kW at I_s = 1020 W/m^2, respectively, a 33% and 300% increase. Where, $\dot{E}_{el}$ at A_{PV}= 100 m² is 65.57 kW at I_s = 5102 W/m^2, up from 51.16 kW at I_s = 3061 W/m^2 and 19.7 kW at I_s = 1020 W/m^2, representing a 28% and 225% increase, respectively. This strong correlation highlights two key points: first, increasing the PV area boosts energy output, and second, solar radiation intensity mainly influences energy production. Figure 7 and Tab. 5

demonstrate that maximizing PV system performance involves optimizing panel area and ensuring maximum sunlight.

Table 4. Influence of cooling air velocity on the different systems' electrical energy productivities at A_{PV}= 60 m², β= -0.3%/°C.

Solar intensity (W/m²)	V_{air} (m/s)	Electrical energy productivity, $E^{\cdot}_{el}$ (kW)			
		PV/HS-I	PV/HS-II	PV/HS-III	PV/HS-IV
1020	0.5	10.95	11.41	11.13	11.32
	1	11.56	11.69	11.61	11.65
	1.5	11.7	11.82	11.77	11.8
	2	11.77	11.87	11.81	11.86
	2.5	11.78	11.91	11.82	11.87
	3	11.82	11.96	11.83	11.88
3061	0.5	24.39	26.48	25.99	26.09
	1	26.7	29.26	28.15	28.33
	1.5	27.9	30.7	29.17	29.1
	2	28.79	30.16	29.82	29.97
	2.5	29.06	30.16	30.11	30.31
	3	29.36	30.47	30.55	30.58
5102	0.5	27.34	28.42	31.38	29.6
	1	32.77	35.37	34.29	35.36
	1.5	36.17	39.34	37.4	38.44
	2	38.07	41.71	39.36	40.46
	2.5	38.87	42.81	40.56	41.25
	3	39.98	43.73	41.49	42.24

Table 5. Influence of photovoltaic area on the different systems' electrical energy productivities at $m^{\cdot}_{air}$= 1.62 kg/s, β= -0.3%/°C.

Solar intensity (W/m²)	A_{PV} (m²)	Electrical energy productivity, $E^{\cdot}_{el}$ (kW)			
		PV/HS-I	PV/HS-II	PV/HS-III	PV/HS-IV
1020	30	5.852	5.909	5.885	5.903
	40	7.802	7.878	7.846	7.87
	50	9.753	9.848	9.808	9.838
	60	11.7	11.82	11.77	11.81
	70	13.65	13.79	13.73	13.77
	80	15.6	15.76	15.69	15.74
	90	17.55	17.73	17.65	17.71
	100	19.51	19.7	19.62	19.68
3061	30	13.95	15.35	14.58	14.55
	40	18.6	20.47	19.44	19.4
	50	23.25	25.58	24.31	24.25
	60	27.91	30.7	29.17	29.1
	70	32.56	35.82	34.03	33.94
	80	37.21	40.93	38.89	38.79
	90	41.86	46.05	43.75	43.64
	100	46.51	51.16	48.61	48.49
5102	30	18.09	19.67	18.7	19.22
	40	24.11	26.23	24.93	25.63
	50	30.14	32.78	31.17	32.03
	60	36.17	39.34	37.4	38.44
	70	42.2	45.9	43.64	44.85
	80	48.23	52.45	49.87	51.25
	90	54.26	59.01	56.1	57.66
	100	60.29	65.57	62.34	64.07

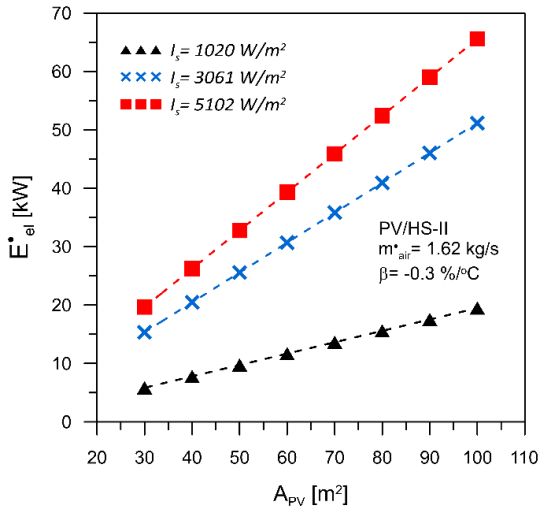

Figure 7. Influence of photovoltaic area on the system's electrical energy productivity at different solar intensities.

APV and β on the system's electrical energy productivity ($\dot{E}_{el}$) at varying sun intensities are shown in Fig. 8: I_s =1020, 3061, and 5102 W/m^2 for PV/HS-II modules. As I_s rises, so does its impact. At low irradiance (I_s =1020 W/m^2), Fig. 8-a shows that the difference between the three β values is minimal. Figure 8-c shows that at high irradiance (I_s = 5102W/m^2), β considerably reduces $\dot{E}_{el}$ from 65.57 kW at β= −0.3%/°C to 40 kW at β= −0.5%/°C, a 40% reduction. Under high solar input circumstances, surface cell temperature management is crucial. In conclusion, increasing PV area increases energy productivity, while minimizing temperature sensitivity (lower β values) is critical for optimal output at higher irradiance levels.

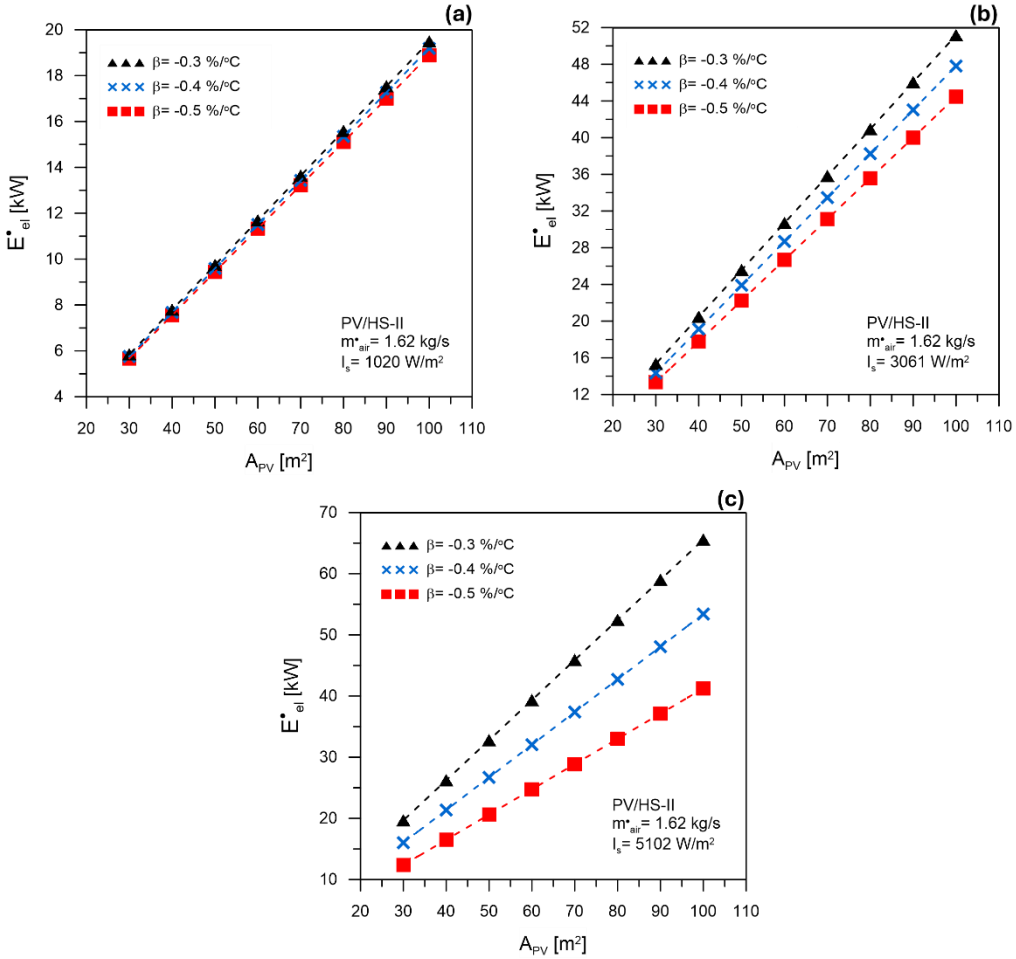

Figure 8. Influence of photovoltaic area on the system's electrical energy productivity at different power temperature coefficients; (a) I_s= 1020 W/m^2, (b) I_s= 3061 W/m^2, (c) I_s= 5102 W/m^2

4.2. Comparison of the electrical and thermal performance of PV/HS-II module with others from the literature

The PV/HS-II module shows improved performance compared to current PV cooling systems, as illustrated in Tab. 6, reaching a peak η_{el} of 19.5%, which significantly surpasses the 7–15% power improvement documented by Liu et al. [42] and the 3% efficiency increase reported by Idoko et al. [44]. The system effectively reduces cell temperature to 26.5°C, exceeding the 10.28°C reduction achieved by Rahman et al.'s finned tube design [45] and matching the 28.038°C reduction of Ahmeda et al.'s optimal module [46]. Unlike the findings of Berghanem et al., which show a 0.5%/°C efficiency decline with rising temperature [43], our design maintains consistent performance even under extreme irradiation levels (5102 W/m²). The 65.57 kW output for a 100 m² system demonstrates greater scalability than Idoko et al.'s 20.96 W improvement [44]. These results establish PV/HS-II as an ideal solution for high-irradiance environments, combining thermal stability, electrical efficiency, and economic viability within a unified system.

Table 6. Comparison of PV/HS-II module with others from the literature

Authors	Type of study	Type of cooling	Cooling technique	Thermal results	Electrical Results
Yanfeng Liu et al. [42]	Numerical & Experimental	Active	Cooling system with various parameters	--	The improved cooling system can increase power generation by 7− 15 %
Benghanem et al. [43]	Experimental	Active	Thermoelectric (TE) as a cooling module in hot climatic conditions	--	The efficiency of solar cells decreases with an increase of their temperature by 0.5 % for each °C increase in temperature.
Linus Idoko et al. [44]	Experimental	Active	Multi-concept cooling techniques (PV + heat sink and water cooling)	Cell surface temperature was reduced to 20 °C	The output increased by 20.96 W, and the efficiency by at least 3 %.
Mohammad Mafizur Rahman et al. [45]	Experimental	Active	Finned tube heat exchanger attached to the back of the photovoltaic panel	Cell surface temperature reduced by 10.28 °C	--
Ahmeda et al. [46]	Numerical & Experimental	Active	PV panel integrated with heat sink modules	Cell surface temperature decreased the cell temperature by 28.038 °C	PVT/HS-3 increased $\Delta\eta_{PV}$ by 14.019 % and $\eta_{rel,enh}$ by 70.095 %
Current Work	Experimental	Active	PV solar panel integrated with heat sink modules	PV/HS-II module reduced the cell surface temperature to 26.5 °C	PV/HS-II module produced maximum output electrical power of 65.57 kW and peak electrical efficiency (η_{el}) of 19.5 %

5. Conclusion and Future Work

This study examined how four unique heat sink designs (PV/HS-I, PV/HS-II, PV/HS-III, and PV/HS-IV) improved the performance of photovoltaic (PV) solar cell modules. The PV/HS-II module was the most successful, with a peak electrical efficiency (η_{el}) of 19.5% at 3 m/s, a 4.25 % improvement over the reference

PV/HS-I design. Thermal analysis showed that raising V_{air} from 0.5 to 3 m/s decreased T_{PV} by 10% (from 29.5 to 26.5 °C) and improved η_{el} and $E^{\bullet}_{el}$ by 5% and 4.7%, respectively, with I_s =1020 W/m^2, A_{PV}= 60 m^2, and β= −0.3%/°C. At V_{air} = 0.5 m/s, PV/HS-I has the lowest η_{el} (≈17.9%), while PV/HS-II has the greatest (≈18.65%). As V_{air} grows to 3 m/s, PV/HS-II gets the maximum η_{el} (≈19.5%). The η_{el} gap between PV/HS-II and PV/HS-IV increased from 0.8% to 1.7% as V_{air} increased from 0.5 to 3 m/s. The study revealed that the increased influence of I_s resulted in a 39.5% decline in η_{el} at 5102 W/m² compared to 1020 W/m², underlining the importance of active cooling for PV modules in high-I_s areas. Scaling effects were noticeable. The peak electrical energy productivity ($E^{\bullet}_{el}$) of a 100 m² PV/HS-II system was 65.57 kW, 225% higher than a 30 m² installation. Lowering the temperature coefficient (β) from -0.5%/°C to -0.3%/°C led to a 40 % increase in $E^{\bullet}_{el}$ at maximum solar irradiation.

Future research should explore hybrid cooling systems that incorporate improved heat sinks, phase-change materials, and AI-driven control to enhance photovoltaic performance in arid environments. Key aspects include analyzing thermal stress effects on module integrity at extreme irradiance levels (e.g., 5102 W/m²) and investigating material deterioration caused by aging, corrosion, and fouling in specific environmental conditions. The trade-off between cooling air velocity, pressure drop, and fan energy consumption must be assessed to determine overall energy benefits. Implementing adaptive airflow management, such as IoT-enabled variable-speed fans, could boost real-time electrical efficiency.

Acknowledgments

This work was funded by the University of Jeddah, Jeddah, Saudi Arabia, under grant No. (UJ-23-DR-81). Therefore, the authors thank the University of Jeddah for its technical and financial support

Nomenclature

A	Area, m^2
A_c	Cross-sectional area, m^2
A_{PV}	Photovoltaic panel area, m^2
$c_{p,a}$	Air specific heat, kJ/kg K
$E^{\bullet}_{el}$	Electrical power, kW
I_s	Total solar intensity, W/m^2
k_{wood}	Wood thermal conductivity, W/m K
$m^{\bullet}_{air}$	Cooling air mass flow rate, kg/s
$N_{p,HS}$	The number of heat sinks in parallel
$N_{s,HS}$	The number of heat sinks in series
$Q^{\bullet}$	Heat capacity, kW
R_t	Total thermal resistance, °C/W
x_i	Wooden box side thickness, m
T	Temperature, °C
T_1	The heat sink's air inlet temperature, °C
T_2	Temperature of the heat sink's air intake, °C
V_{air}	Cooling air velocity, m/s

Greek symbols

β	Power temperature coefficient, %/°C
η_{el}	Electrical efficiency, %
ρ_{air}	Air density, kg/m^3

Subscript

a	Air
b	Base
el	Electrical
H	Heat sink heater

HS	Heat sink
i= 1, 2, 3, …	Index of thermocouples positions
L	Losses
o	Ambient
ref	Reference
p	Parallel
s	Surface

Abbreviations

Conv/div	Convergence / Divergence
DAQ	Data Acquisition System
EES	Engineering Equation Solver
HS	Heat sink
NIST	National Institute of Standards and Technology
PCMs	Phase Change Materials
PV	photovoltaic
PVT	photovoltaic/thermal

References

[1] Olabi, A.G., Elsaid, K., Obaideen, K., Abdelkareem, M.A., Rezk, H., Wilberforce, T., Maghrabie, HM., Enas taha sayed, Renewable energy systems: comparisons, challenges and barriers, sustainability indicators, and the contribution to UN sustainable development goals, Int. J. Thermofluids 20 (2023), 100498. https://doi.org/10.1016/j.ijft.2023.100498

[2] Obaideen, K., Nooman AlMallahi, M., Alami, A.H., Ramadan, M., Abdelkareem, M.A., Shehata, N., Olabi, A., On the contribution of solar energy to sustainable developments goals: case study on Mohammed bin Rashid Al Maktoum solar park, Int. J. Thermofluids 12 (2021) 100123. https://doi.org/10.1016/j.ijft.2021.100123

[3] Aljaghoub, H., Abumadi, F., AlMallahi, M.N., Obaideen, K., Alami, A.H., Solar PV cleaning techniques contribute to sustainable development goals (SDGs) using multi-criteria decision-making (MCDM): assessment and review, Int. J. Thermofluids 16 (2022) 100233, https://doi.org/10.1016/j.ijft.2022.100233

[4] Almadhhachi, M., Seres, I., Farkas, I., Electrical power harvesting enhancement of PV module by a novel hemispherical configuration, Int. J. Thermofluids 20 (2023) 100460, https://doi.org/10.1016/j.ijft.2023.100460

[5] Salameh, W., Faraj, J., Khaled, M., Numerical study of cooling photovoltaic panels with air exhausted from industrial systems: comparisons and innovative configurations, Int. J. Thermofluids 20 (2023) 100493. https://doi.org/10.1016/j.ijft.2023.100493

[6] Radwan, A., Mahmoud, M., Olabi, A., Rezk, A., Maghrabie, H.M., Abdelkareem, M.A., Thermal comparison of mono-facial and bi-facial photovoltaic cells considering the effect of TPT layer absorptivity, Int. J. Thermofluids 18 (2023) 100306. https://doi.org/10.1016/j.ijft.2023.100306

[7] Salehi, R., Jahanbakhshi, A., Ooi, J.B., Rohani, A., Golzarian, M.R., Study on the performance of solar cells cooled with heatsink and nanofluid added with aluminum nanoparticle, Int. J. Thermofluids 20 (2023) 100445. https://doi.org/10.1016/j.ijft.2023.100445

[8] Alsaqoor, S., Alqatamin, A., Alahmer, A., Nan, Z., Al-Husban, Y., Jouhara, H., The impact of phase change material on photovoltaic thermal (PVT) systems: a numerical study, Int. J. Thermofluids 18 (2023) 100365. https://doi.org/10.1016/j.ijft.2023.100365

[9] Bhakre, S.S., Sawarkar, P.D., Kalamkar, V.R., Performance evaluation of PV panel surfaces exposed to hydraulic cooling – A review, Sol. Energy 224 (2021) 1193–1209. https://doi.org/10.1016/j.energy.2022.124654

[10] Sheikh, Y., Jasim, M., Qasim, M., Qaisieh, A., Hamdan, M.O., Abed, F., Enhancing PV solar panel efficiency through integration with a passive Multi-layered PCMs cooling system: a numerical study, Int. J. Thermofluids 23 (2024) 100748. https://doi.org/10.1016/j.ijft.2024.100748

[11] Habchi, C., Bou-Mosleh, C., Khaled, M., An experimental analysis of a hybrid photovoltaic thermal system through parallel water pipe integration, Int. J. Thermofluids 21 (2024) 100538. https://doi.org/10.1016/j.ijft.2023.100538

[12] Siah Chehreh Ghadikolaei, S., Solar photovoltaic cells performance improvement by cooling technology: an overall review, Int. J. Hydrog. Energy 46 (18) (2021) 10939–10972. https://doi.org/10.1016/j.ijhydene.2020.12.164

[13] Cui, Y., Zhu, J., Zhang, F., Shao, Y., Xue, Y., Current status and future development of hybrid PV/T system with PCM module: 4E (energy, exergy, economic, and environmental) assessments, Renew. Sustain. Energy Rev. 158 (2022) 112147. https://doi.org/10.1016/j.rser.2022.112147

[14] Madhi, H., Aljabair, S., Imran, A.A., A review of photovoltaic/thermal system cooled using mono and hybrid nanofluids, Int. J. Thermofluids 22 (2024) 100679. https://doi.org/10.1016/j.ijft.2024.100679

[15] Dida, M., Boughali, S., Bechki, D., Bouguettaia, H., Experimental investigation of a passive cooling system for photovoltaic modules efficiency improvement in hot and arid regions, Energy Convers. Manag. 243 (2021) 114328. https://doi.org/10.1016/j.enconman.2021.114328

[16] Suresh, A.K., Khurana, S., Nandan, G., Dwivedi, G., Kumar, S., Role on nanofluids in cooling solar photovoltaic cell to enhance overall efficiency, Mater. Today: Proc. 5 (9) (2018), 20614–20620. https://doi.org/10.1016/j.matpr.2018.06.442

[17] Ghadiri, M., Sardarabadi, M., Pasandideh-fard, M., Moghadam, A.J., Experimental investigation of a PVT system performance using nano ferrofluids, Energy Convers. Manage. 103 (2015), 468–476. https://doi.org/10.1016/j.enconman.2015.06.077

[18] Idoko, L., Anaya-Lara, O., McDonald, A., Enhancing PV modules efficiency and power output using multi-concept cooling technique, Energy Rep. 4 (2018), 357–369. https://doi.org/10.1016/j.egyr.2018.05.004

[19] Omisanya, M.I., Hamzat, A.K., Adedayo, S.A., Adediran, I.A., Asafa, T.B., Enhancing the thermal performance of solar collectors using nanofluids, IOP Conf. Ser. Mater. Sci. Eng. 805 (1) (2020), 012015. https://doi.org/10.1016/j.csite.2025.106460

[20] Siecker, J., Kusakana, K., Numbi, E.B., A review of solar photovoltaic systems cooling technologies, Renew. Sustain. Energy Rev. 79 (2017), 192–203. https://doi.org/10.1016/j.rser.2017.05.053

[21] Cătălin George Popovici, Sebastian Valeriu Hudișteanua, Theodor Dorin Mateescu, Nelu-Cristian Chereches, Efficiency improvement of photovoltaic panels by using air cooled heat sinks, Energy Procedia 85 (2016) 425 – 432. https://doi.org/10.1016/j.egypro.2015.12.223

[22] Mazón-Hernández, R., García-Cascales, J.R., Vera-García, F., Káiser, A.S., Zamora, B., Improving the electrical parameters of a photovoltaic panel by means of an induced or forced air stream, Int. J. Photoenergy (2013). https://doi.org/10.1155/2013/830968

[23] Golzari, S., Kasaeian, A., Amidpour, M., Nasirivatan, S., Mousavi, S., Experimental investigation of the effects of corona wind on the performance of an air-cooled PV/T., Renew Energy 127 (2018), 284–297. https://doi.org/10.1016/j.renene.2018.04.029

[24] Kaiser, A.S., Zamora, B., Mazón, R., García, J.R., Vera, F., Experimental study of cooling BIPV modules by forced convection in the air channel, Appl. Energy 135 (2014), 88–97. https://doi.org/10.1016/j.apenergy.2014.08.079

[25] Teo, H.G., Lee, P.S., Hawlader, M.N.A., An active cooling system for photovoltaic modules, Appl. Energy 90 (1) (2012), 309–315. https://doi.org/10.1016/j.apenergy.2011.01.017

[26] Soliman, A.M., Hassan, H., Ookawara, S., An experimental study of the performance of the solar cell with heat sink cooling system, Energy Procedia 162 (2019), 127–135. https://doi.org/10.1016/j.egypro.2019.04.014

[27] Arifin, Z., Tjahjana, D.D.D.P., Hadi, S., Rachmanto, R.A., Setyohandoko, G., Sutanto, B., Numerical and experimental investigation of air cooling for photovoltaic panels using aluminum heat sinks, Int. J. Photoenergy (2020). https://doi.org/10.1155/2020/1574274

[28] A. Almuwailhi, O. Zeitoun, Investigating the cooling of solar photovoltaic modules under the conditions of Riyadh, Journal of King Saud University – Engineering Sciences 35 (2023) 123–136. https://doi.org/10.1016/j.jksues.2021.03.007

[29] Ahssan M.A. Alshibil, Piroska Vig, Istvan Farkas, Performance enhancement attempts on the photovoltaic/thermal module and the sustainability achievements: A review, Energy 304 (2024) 132099. https://doi.org/10.1016/j.energy.2024.132099

[30] Ihsan Okta Harmailil, Sakhr M., Sultan, Tso, C.P., Ahmad Fudholi, Masita Mohammad, Adnan Ibrahim, A review on recent photovoltaic module cooling techniques: Types and assessment methods, Results in Engineering 22 (2024) 102225. https://doi.org/10.1016/j.rineng.2024.102225

[31] Mahmoud M. Abd-Elhady, Mohab A. Elhendawy, Muhannad S. Abd-Elmajeed, Rahaf B. Rizk, Enhancing photovoltaic systems: A comprehensive review of cooling, concentration, spectral splitting, and tracking techniques, Next Energy 6 (2025) 100185. https://doi.org/10.1016/j.nxener.2024.100185

[32] Mohamad Abou Akrouch, Khaled Chahine, Jalal Faraj, Farouk Hachem, Cathy Castelain, Mahmoud Khaled, Advancements in cooling techniques for enhanced efficiency of solar photovoltaic panels: A detailed comprehensive review and innovative classification, Energy and Built Environment 6 (2025) 248-276. https://doi.org/10.1016/j.enbenv.2023.11.002

[33] Al-Waeli, Ali H.A., Kazem, Hussein A., Yousif, Jabar H., Chaichan, Miqdam T., Sopian, Kamaruzzaman, Mathematical and neural network models for predicting the electrical performance of a PV/T system, Int. Journal of Energy Research (2019) 1-18. https://doi.org/10.1002/er.4807

[34] Kazem, Hussein A., Al-Waeli, Ali H.A., Chaichan, Miqdam T., Sopian, Kamaruzzaman, Numerical and experimental evaluation of nanofluids based photovoltaic/thermal systems in Oman: Using silicone-carbide nanoparticles with water-ethylene glycol mixture, Case Studies in Thermal Engineering 26 (2021) 101009. https://doi.org/10.1016/j.csite.2021.101009

[35] Djordjevic, Stefan N., Krstic, Marko S., Pantic, Lana S., Radonjic, Ivana S., Mancic, Marko V., Begovic, Veljko S., Gocic, Sasa R., Radovanovic, Branka G., Enhancement of pv panel's power using closed back side cooling system and numerical simulation, Thermal Science OnLine-First Issue 00 (2025) 52-52. https://doi.org/10.2298/TSCI241218052D

[36] Muniy, Srilasri and Narayanasamy, Stalin, Experimental analysis on the performance of photovoltaic module with al2o3 deionized water nanofluid, Thermal Science 28 (2024) 1A 357-364. https://doi.org/10.2298/TSCI230829268M

[37] Hasan, A., Sarwar, J., Effect of fin spacing and length on the thermal performance of heat sinks in PVT systems, Renewable Energy Journal 45 (2017), 123-134. doi:10.1088/1755-1315/1281/1/012059

[38] Kumar, R., & Singh, S., Optimization of heat sink designs for enhanced cooling in photovoltaic-thermal systems, Energy Conversion and Management 180 (2019) 789-801. https://doi.org/10.1016/j.enbuild.2022.112274

[39] Klein, S.A., Engineering Equation Solver (EES) for Microsoft Windows Operating Systems: Academic Professional Version. F-chart Software, Medison, WI, USA, 2012. Available online: http://www.fchart.com (accessed on 5 February 2025).

[40] Moffat, R.J., Describing the uncertainties in experimental results, Exp. Therm. Fluid Sci 1 (1) (1988) 3–17. https://doi.org/10.1016/0894-1777(88)90043-X

[41] Taylor, J.R., An Introduction to Error Analysis: The Study of Uncertainties in Physical Measurements, 2nd ed., University Science Books, Sausalito, CA, 1997. ISBN: 1940380081, 9781940380087

[42] Madhu Sharma, Kamal Bansal, Dharam Buddhi, Real time data acquisition system for performance analysis of modified PV module and derivation of cooling coefficients of electrical parameters, Procedia Comput. Sci. 48 (2015) 582–588. https://doi.org/10.1016/j.procs.2015.04.139

[43] Benghanem, M., Al-Mashraqi, A.A., Daffallah, K.O., Performance of solar cells using thermoelectric module in hot sites, Renew. Energy 89 (2016) 51–59. https://doi.org/10.1016/j.renene.2015.12.011

[44] Linus Idoko, Olimpo Anaya-Lara, Alasdair McDonald, Enhancing PV modules efficiency and power output using multi-concept cooling technique, Energy Rep. 4 (2018) 357–369. https://doi.org/10.1016/j.egyr.2018.05.004

[45] Elnozahy, A., Abd-Elbary, H., Abo-Elyousr, F.K., Efficient energy harvesting from PV Panel with reinforced hydrophilic nano-materials for eco-buildings, Energy Built Environ. 5 (2024) 393–403. https://doi.org/10.1016/j.enbenv.2022.12.001

[46] Anas Ahmed, Fouda, A., Elattar, H.F., Khaled Alnamasi, Alsharif Abdullah, M.A., Advancing photovoltaic thermal module efficiency through optimized heat sink designs, Applied Thermal Engineering 271 (2025) 126241. https://doi.org/10.1016/j.applthermaleng.2025.126241

RECEIVED DATE: 01.06.2025
DATE OF CORRECTED PAPER: 28.06.2025
DATE OF ACCEPTED PAPER: 05.08.2025